Article citation info:
Wang F. Improvement of the wavelet transform filtering algorithm with threshold denoising method. Diagnostyka. 2025;26(3):2025309. https://doi.org/10.29354/diag/209428.

DIAGNOSTYKA, 2025, Vol. 26, No. 3

e-ISSN 2449-5220
DOI: 10.29354/diag/209428

IMPROVEMENT OF THE WAVELET TRANSFORM FILTERING ALGORITHM WITH THRESHOLD DENOISING METHOD

Fan WANG

Training Technology and Equipment Management Center, Shijiazhuang College of Applied Technology, Shijiazhuang, 050800, China
Corresponding author, e-mail: mean_wangf@outlook.com

Abstract

In recent years, the wavelet transform filtering algorithm has attracted significant attention due to widespread applications in signal denoising. However, its fixed threshold method has limitations, such as constrained denoising performance and loss of signal details, which requires improvement to adapt to complex noise environments. To address this issue, a wavelet transforms filtering algorithm combining adaptive thresholding and an improved threshold function is proposed. The algorithm dynamically calculates thresholds based on the statistical properties of the signal and employs a continuously differentiable threshold function to balance denoising and signal fidelity. Experimental tests on simulated signals with varying noise levels and real-world signals show that the improved algorithm achieves an SSIM index of 0.942, the closest to the original image, preserving image details and textures to the greatest extent. In denoising house images, the GAPT-Wavelet method clearly preserves the contours and textures of the house, with a PSNR of 87.90 dB and an MSE of 0.021 dB. When the maximum data size n=800, the algorithm's runtime is 46 seconds, maintaining a fast response time. The study has shown that the improved algorithm outperforms traditional methods in terms of denoising performance, computational efficiency, and adaptability, demonstrating significant potential for practical applications in scenarios such as medical image denoising, engineering equipment fault diagnosis, and industrial signal monitoring, thereby highlighting its important practical significance in the fields of engineering and technical diagnostics.

Keywords: Wavelet Transform Filtering Algorithm; Adaptive Thresholding; Fast and Flexible Denoising Network; Generative Adversarial Networks; Signal Denoising; Threshold Function

1. INTRODUCTION

With the increasing demands for signal quality in fields such as communications, healthcare, and seismic monitoring, signal denoising technology has become crucial for improving data quality and ensuring the effectiveness of subsequent processing. In recent years, the Wavelet Transform Filtering Algorithm (WTFA) has been widely applied in various signal processing tasks due to its advantages in multi-scale analysis and efficient denoising [1]. Wavelet transform can effectively decompose signals, extract features from different frequency ranges, and possesses good time-frequency localization properties [2]. However, traditional WTFA often relies on fixed threshold strategies, which show certain limitations in complex noise environments. This can lead to restricted denoising performance and often fails to preserve signal details adequately [3]. The adaptive thresholding method can dynamically adjust thresholds based on the statistical properties of different signals, allowing for more accurate differentiation between signal and noise, and avoiding the inefficiency of fixed thresholds in changing noise environments [4]. By adjusting the threshold function, signal details can be effectively preserved while denoising, thus enhancing denoising performance and signal quality [5]. Therefore, this study proposes a WTFA based on adaptive thresholding and an improved threshold function. The innovation of this algorithm lies in the introduction of a dynamic threshold adjustment mechanism, which combines the statistical characteristics of the signal and multi-scale analysis to overcome the limitations of traditional fixed threshold methods, improving the algorithm's adaptability and denoising performance. This improved method is flexible in handling different noise levels and signal characteristics, offering high computational efficiency and better denoising performance. It provides new ideas and technical solutions for the field of signal denoising.

Received 2024-03-13; Accepted 2025-08-12; Available online 2025-08-12

© 2025 by the Authors. Licensee Polish Society of Technical Diagnostics (Warsaw. Poland). This article is an open access article distributed under the terms and conditions of the Creative Commons Attribution (CC BY) license (http://creativecommons.org/licenses/by/4.0/).

2. RELATED WORK

The WTFA, due to its superior time-frequency localization properties, performs excellently in handling signals with multi-scale features and complex noise. It is widely applied in fields such as signal denoising, image processing, and speech recognition [6]. Molaei et al. addressed the issue of incompatibility with Fourier transform in 3D near-field dual-station microwave imaging caused by physical layer compression and non-uniform radiation patterns in dynamic metasurface antennas. They proposed a Fourier transform-based imaging algorithm, and experimental results demonstrated its excellent performance in numerical simulations [7]. Jiang et al. tackled the problem of fixed time windows in S-transform, which leads to limited time-frequency resolution and poor energy concentration in seismic signal analysis. They proposed an adaptive generalized S-transform algorithm based on a novel generalized Gaussian window function. Experimental results showed that this method improved time-frequency resolution and energy concentration in seismic signal analysis [8]. Li et al. addressed the problem of difficulty in identifying the first wave in microseismic records due to the mixture of high- and low-frequency noise. They proposed an innovative threshold denoising method based on discrete wavelet transform. This method demonstrated higher denoising efficiency in various contrast tests and significantly enhanced the clarity of the first wave in actual microseismic records [9]. Tian et al. solved the issue of low reconstruction accuracy due to the limited characterization ability of discrete cosine transform in the electro-photoplethysmographic inference of standard electrocardiogram. They proposed an improved framework based on cross-domain joint dictionary learning and label consistency, and experimental results achieved Pearson correlation coefficients of 0.88 and 0.92 on two benchmark datasets [10]. Yao et al. addressed the low computational efficiency of traditional supervised descent methods in electromagnetic inverse scattering problems. They proposed an enhanced supervised descent learning framework combining complex-valued deep convolutional neural networks and semantic segmentation models. Experimental results showed that this framework significantly reduced computation time and achieved real-time imaging. [11].

With the increasing demand for signal processing, threshold denoising methods, as one of the classic denoising techniques, have gradually overcome the limitations of traditional fixed threshold methods in complex noise environments by introducing adaptive adjustment mechanisms and optimizing threshold functions. This has effectively improved denoising performance and signal fidelity [12]. For example, Peng et al proposed a fault diagnosis method for air compressors based on improved Complete Ensemble Empirical Mode Decomposition with Adaptive Noise (ICEEMDAN) combined with wavelet threshold denoising, and further constructed a fault identification model using MPGA-SVM. Compared with the CEEMDAN plus wavelet threshold approach, the proposed joint denoising method improved the signal-to-noise ratio by 6.5% and reduced the mean squared error by 16.1%, while the MPGA-SVM model achieved a fault diagnosis accuracy of 98.33% [13]. Wang et al. addressed the problem that traditional vibration-based fault diagnosis is susceptible to noise interference, and proposed a fault diagnosis method based on time-shift denoising and discrete wavelet transform-enhanced conditional domain adaptation using motor stator current signals. Experimental results showed that this method achieved a maximum diagnostic accuracy of 93.94% across two public datasets and one real-world dataset [14]. Iqbal et al. addressed the challenge of noise suppression in seismic signal processing by proposing an intelligent denoising framework, DeepSeg, based on deep convolutional neural networks. The DeepSeg model was trained using only synthetic seismic data without relying on real data, making it highly adaptable and showing potential in fields such as seismic imaging, environmental noise preprocessing, and microseismic event monitoring [15]. Yao et al. addressed the issue of decreased fault diagnosis accuracy in high-noise industrial environments by proposing an intelligent bearing fault diagnosis framework incorporating instance-enhanced batch normalization, improved channel attention blocks, and a location-focused soft threshold denoising structure. Experiments conducted on three public datasets validated the effectiveness and robustness of this method for fault identification under high-noise industrial scenarios [16]. Li et al. tackled the challenge of accurately identifying bearing faults in CNC machine tool spindle systems operating under high-noise conditions by introducing a fault diagnosis method combining deep residual shrinkage networks with a Transformer architecture. Experimental results demonstrated that this method achieved a diagnostic accuracy of at least 98% under various SNR conditions [17].

In summary, current research indicates that, although WTFA and threshold denoising methods have made significant progress in various signal processing applications, existing studies have generally relied on fixed threshold or simple adaptive threshold strategies. These methods fail to fully account for the dynamic changes in signal characteristics under complex noise environments, leading to certain limitations in denoising performance and signal detail preservation. To address the issues, this study proposes a wavelet transform filtering algorithm based on an adaptive thresholding method and an improved threshold function (Gaussian Adaptive Thresholding and GAN-FFDNet-based Wavelet, GAPT-Wavelet), with its innovations primarily reflected in several aspects. For the first time, a Gaussian adaptive thresholding

scheme based on statistical characteristics is integrated with a Fast and Flexible Denoising Network (FFDNet) and Generative Adversarial Networks (GAN), enhancing the adaptability of the threshold through deep neural networks and enabling dynamic adjustment to local signal characteristics under complex noise environments. The study employs a continuously differentiable improved threshold function to optimize the balance between denoising and signal fidelity, significantly improving the preservation of signal details. The proposed framework demonstrates strong generalizability and application potential in various typical real-world scenarios such as medical image processing, seismic signal denoising, and industrial equipment monitoring. Although this method achieves notable improvements in denoising performance and detail preservation, the introduction of deep learning structures inevitably increases the computational complexity and resource consumption compared with traditional methods. Future work may further optimize the model in terms of lightweight design and real-time performance to expand its applicability to large-scale real-time applications.

3. WTFA BASED ON GAUSSIAN ADAPTIVE THRESHOLDING AND AN IMPROVED THRESHOLD FUNCTION

3.1 Gaussian adaptive thresholding based on the combination of FFDNet and GAN

Adaptive thresholding methods dynamically adjust thresholds to adapt to various noise environments, enhancing the flexibility and performance of thresholding techniques in complex signal processing tasks, and proving suitable for improving WTFA [18-19]. FFDNet is a deep learning-based denoising network, directly accepts noise level information and adjusts thresholds during the denoising process based on noise intensity, effectively addressing these limitations. It primarily employs convolutional neural networks for image or signal denoising [20]. The FFDNet architecture is illustrated in figure 1.

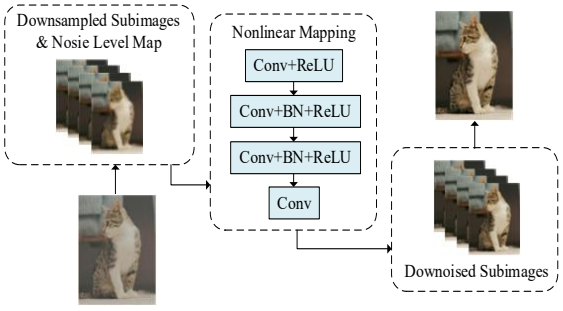

Fig. 1. FFDNet structure diagram

Figure 1 shows the operational architecture of FFDNet. The network's core component, the nonlinear mapping module, includes multiple layers of convolution operations and activation functions. The first layer applies convolution and ReLU activation. Two subsequent layers combine convolution with batch normalization and ReLU activation, followed by a final convolutional layer that generates denoised features. The nonlinear mapping module processes the input and outputs denoised sub-images. The reconstruction process then combines these sub-images into a complete denoised image. FFDNet focuses on using the input noisy signal and noise standard deviation for denoising, as described in equation (1) [21].

$$x = G(y,\sigma) \qquad (1)$$

In equation (1), x represents the denoised signal, y denotes the input signal, σ stands for the noise standard deviation, and G refers to the FFDNet denoising network. During training, FFDNet adopts the L2 loss function, minimizing the Mean Squared Error (MSE) between the denoised result and the ground truth signal. The loss function is described in equation (2).

$$L_{FFDNet} = \mathrm{E}_{y\sim p_y}[\|x - x_{true}\|_2^2] \qquad (2)$$

In equation (2), x_{true} represents the true signal. FFDNet uses a residual network structure, where each layer applies convolutional operations to extract features from the signal and enhances the learning effect through residual connections. However, the traditional approach used by FFDNet mainly relies on convolutional network-based noise prediction, which struggles with detail recovery when generating higher-quality images. Therefore, GAN is introduced to enhance the recovery of image details and textures [22]. When combining FFDNet with GAN, the goal is to use GAN to improve the details of the denoised signal and then use FFDNet to perform the denoising. The integrated network can generate more natural and realistic signals. For the structure and objective of the combined network, the generator part uses FFDNet for initial denoising of the noisy signal, producing a denoised image or signal. The denoised signal expression is shown in equation (3) [22] .

$$G(y,\sigma) = FFDNet(y,\sigma) \qquad (3)$$

In equation (3), y represents the noisy input, σ is the standard deviation of the noise, and $G(y,\sigma)$ is the denoised signal output by the generator. The objective of the discriminator is to determine whether the signal output by the generator is close to the real signal, thereby helping the generator improve the denoising effect. The discriminator distinguishes between the generated signal and the real signal by outputting a probability value, D . The expression is shown in equation (4).

$$D(x) = \sigma(W_d \cdot x + b_d) \qquad (4)$$

In equation (4), W_d and b_d represent the weights and biases of the discriminator, σ is the Sigmoid activation function, and $D(x)$ indicates the probability that the input signal is a real signal.

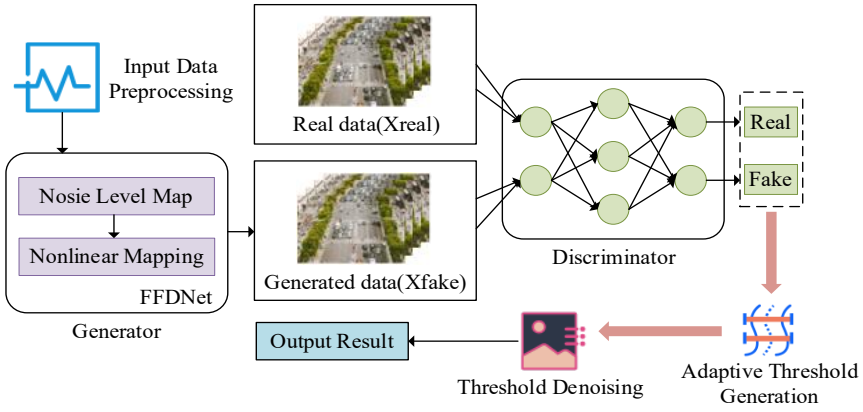

Fig. 2. Operational structure of the improved adaptive thresholding method

The training objective of GAN is to minimize the adversarial loss between the generator and the discriminator. The goal of the generator is to deceive the discriminator into believing that the generated signal comes from a real signal. The loss functions of the generator and discriminator are shown in equation (5).

$$\begin{cases} L_G = \mathrm{E}_{y\sim p_y}[\log(1-D(G(y,\sigma)))] \\ L_D = \mathrm{E}_{x\sim p_x}[\log D(x)] + E_{y\sim p_y}[\log(1-D(G(y,\sigma)))] \end{cases} \quad (5)$$

In equation (5), p_x represents the distribution of the real signal, p_y represents the distribution of the noisy signal, D is the discriminator, and L_G and L_D are the adversarial losses of the generator and discriminator. The total loss function is expressed in equation (6).

$$L_{total} = L_{FFDNet} + L_G + L_D \quad (6)$$

In equation (6), L_{FFDNet} represents the traditional denoising loss. The total loss of the network training is a weighted combination of the traditional denoising loss, generator loss, and discriminator loss. The total loss function ensures that the generator learns to recover clearer signals from noisy signals, while the discriminator distinguishes the differences between noise and real signals as much as possible. The operational architecture of the integrated adaptive thresholding method with FFDNet and GAN is shown in figure 2.

As shown in figure 2, the method first normalizes the input noisy image or signal and generates the corresponding noise level map. Then, the generator part uses FFDNet for initial denoising, while the discriminator is responsible for distinguishing the differences between the output of the generator and the real image. The entire training process optimizes the generated adaptive threshold by combining FFDNet's noise level prediction ability with GAN's generative capability. This threshold adjusts based on global noise level predictions and feature map distributions to adapt to the noise characteristics of different regions of the image. Finally, by using the adaptive threshold to denoise the high-frequency components and preserve the key information in the low-frequency components, the method outputs an optimized high-quality denoised image or signal, achieving the goal of maximizing noise removal while retaining image details.

3.2 Threshold function based on Gaussian processes and its improvement on WTFA

WTFA performs multi-resolution decomposition of the signal to extract different frequency components, enabling effective separation of noise and precise signal reconstruction. It is an efficient tool widely used for denoising and feature extraction. The operational structure of WTFA is shown in figure 3.

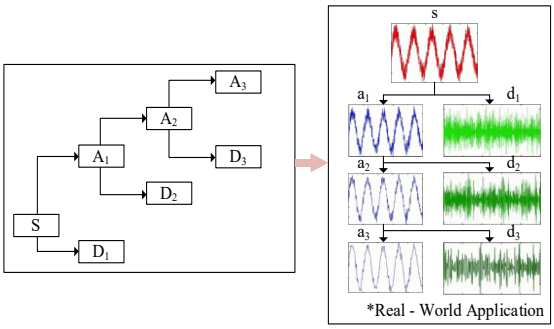

Fig. 3. The operational structure of WTFA

Figure 3 illustrates the structure of WTFA and its signal processing example in practical applications. WTFA first decomposes the input signal S and progressively breaks it down into low-frequency components (A) and high-frequency components (D) according to the decomposition levels. This decomposition can continue deeper, with each level producing more refined frequency bands. The right side shows the corresponding time-domain signals of each layer's decomposition result in practical applications. The low-frequency components retain the overall trend of the signal, while the high-frequency components capture the rapid variations of the signal. By such decomposition and reconstruction, the algorithm effectively extracts different frequency characteristics of the signal, achieving goals such as filtering, denoising, or

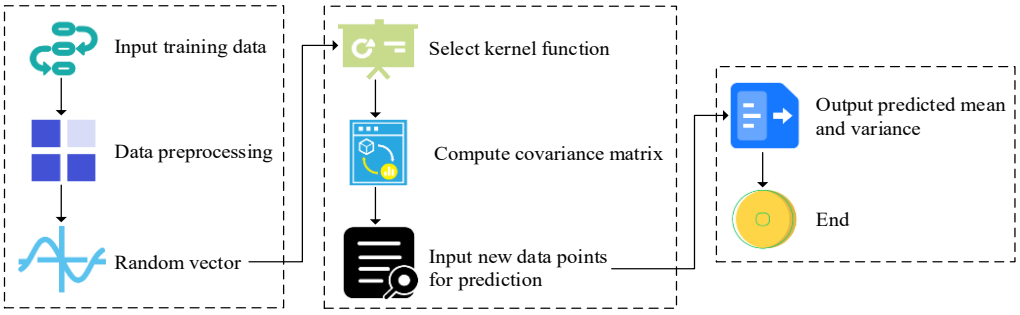

Fig 4. Gaussian regression operational flowchart

feature extraction. By integrating FFDNet and GAN's adaptive thresholding method, the flexibility and adaptability of threshold computation can be enhanced. Building on this, improving the threshold function by introducing a more flexible nonlinear adjustment mechanism enables more precise adaptation to different noise characteristics, thereby improving denoising performance and strengthening WTFA's ability to preserve signals in complex noise environments. The introduction of Gaussian Process (GP) provides more flexible nonlinear modeling capability for the improved threshold function, allowing the threshold function to dynamically adjust based on the statistical characteristics of the data. GP, as a powerful non-parametric method, has a core advantage in inferring through the covariance structure between data without relying on explicit model assumptions [23]. The expression of GP is shown in equation (7).

$$\begin{cases} f(x) \sim \varsigma\rho(m(x), k(x,x')) \\ m(x) = \mathrm{E}[f(x)] \\ k(x,x') = \sigma^2 + \theta|x - x'| \end{cases} \tag{7}$$

In equation (7), $f(x)$ represents a random function defined in the input space x, $\varsigma\rho(m(x), k(x,x'))$ indicates that this function is a GP, with mean function $m(x)$ and covariance function $k(x,x')$. x and x' are points in the input space, σ^2 represents the noise variance. In GP, assume a training dataset $Data = \{X, y\}$, where $X = \{x_1, x_2, \cdots, x_n\}$ is the input data and $y = \{y_1, y_2, \cdots, y_n\}$ is the corresponding output data, which are also the observations. The predicted result obtained through GP regression is shown in equation (8).

$$\begin{cases} p(y_* \mid X, y, x_*) = \mathrm{N}(\mu_*, \sigma_*^2) \\ \mu_* = k(x_*, X) \cdot (K(X,X) + \sigma^2 I)^{-1} y \\ \sigma_*^2 = k(x_*, x_*) - k(x_*, X) \cdot (K(X,X) + \sigma^2 I)^{-1} k(X, x_*) \end{cases} \tag{8}$$

In equation (8), x_* and y_* represent the predicted new test points and the corresponding outputs, respectively, μ_* and σ_*^2 represent the predicted mean and variance, respectively. When processing signals in non-stationary and complex noise environments, using a GP-based threshold function can improve the performance of traditional hard and soft thresholding methods. The typical definition of the hard threshold function is shown in equation (9).

$$T_{hard}(x, \lambda) = \begin{cases} x, & if\ |x| > \lambda \\ 0, & otherwise \end{cases} \tag{9}$$

In equation (9), x represents the signal coefficients, and λ represents the set threshold. Based on equations (7) to (9), the operational flow of GP regression is shown in figure 4.

From figure 4, it can be seen that Gaussian regression consists of three main steps. First, the training data is input and preprocessed to generate random vectors. Next, an appropriate kernel function is chosen, and the covariance matrix is calculated. New data points are then input for prediction, and the model outputs the predicted mean and variance. Finally, the GP regression process is completed. The entire process combines the kernel function and covariance matrix, fully utilizing the properties of Gaussian distributions for regression modeling and prediction. The main issue with the hard thresholding function is that when the coefficient x approaches zero, it causes signal discontinuities, leading to artifacts or ringing effects. To address this, the GP-based hard thresholding function introduces noise covariance estimates, allowing the threshold to adapt to the local features of the signal. The improved hard thresholding function is shown in equation (10).

$$T_{GP-hard}(x, \lambda, \sigma) = \begin{cases} x, & if\ |x| > \lambda \cdot \sigma \\ 0, & otherwise \end{cases} \tag{10}$$

In equation (10), λ is the parameter controlling the threshold, and σ is the signal noise standard deviation estimated by GP. In this case, the threshold dynamically depends on the noise estimate, allowing it to adaptively adjust in different noise environments, thereby better preserving the signal details. The soft thresholding function is improved using the same principle, and the definition of the soft thresholding function is shown in equation (11).

$$T_{soft}(x, \lambda) = \begin{cases} x - \lambda, & if x > \lambda \\ x + \lambda & if x < -\lambda \\ 0, & otherwise \end{cases} \tag{11}$$

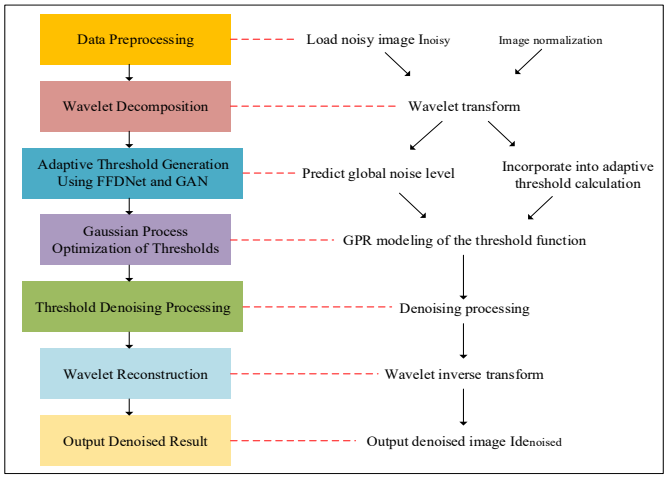

Fig. 5. GAPT-Wavelet operation diagram

In equation (11), the drawback of the soft thresholding function is that it compresses the signal amplitude, especially low-amplitude signals that may be excessively suppressed. To prevent an overall reduction in the signal amplitude, an adaptive threshold can be introduced through GP, so that each signal coefficient is smoothly adjusted based on its local statistical characteristics. The improved function expression is shown in equation (12).

$$T_{GP-soft}(x,\lambda,\sigma)=\begin{cases} x-\lambda\cdot\sigma, & if\ |x|>\lambda\cdot\sigma \\ 0, & otherwise \end{cases} \tag{12}$$

In equation (12), λ and σ are jointly estimated by the GP model. GP is not only used for noise modeling of the signal but also for dynamically adjusting the selection of the threshold, ensuring the authenticity of the signal and the preservation of its details during the denoising process. The final operation process of GAPT-Wavelet is shown in figure 5.

Figure 5 shows the operation process of GAPT-Wavelet. GAPT-Wavelet first preprocesses the noisy image, including loading and normalizing the image, and then performs wavelet transform to decompose the image and extract different frequency components. Next, it uses FFDNet and GAN to generate adaptive thresholds, combines global noise level predictions, and calculates the adaptive thresholds. Subsequently, GP is used to model and optimize the threshold function, generating the final threshold. The high-frequency components are filtered through threshold denoising to remove noise. Finally, an inverse wavelet transform is applied to reconstruct the image, and the denoised image result is output. The entire process integrates deep learning and probabilistic modeling, which enhances the denoising effect and image quality.

4. PERFORMANCE VALIDATION AND COMPARISON OF GAPT-WAVELET

4.1 Verification of GAPT-Wavelet's denoising effect

To verify the performance of the improved WTFA, a series of detailed experimental setups were established. The system used an Intel Core i7 CPU, an NVIDIA RTX 3060 GPU, 16GB of RAM, and a Windows 10 operating system. The programming language Python 3.8, PyTorch 1.10+ framework, and PyWavelets and OpenCV platforms were used, with the Kodak24 image dataset selected. GAPT-Wavelet was compared with the classical Gaussian Filtering Algorithm (GFA), standard WTFA, and Noise2Noise in terms of performance, primarily focusing on denoising effectiveness and computational efficiency. The SSIM index obtained from the experiments are shown in figure 6.

As shown in figure 6(a), the SSIM index of GAPT-Wavelet was 0.942, which was the closest to the original image, indicating that it achieved the best denoising performance with the maximum preservation of image details and textures. In contrast, Noise2Noise had an SSIM index of 0.874, which was second-best but still showed some loss of details. The WTFA image was blurry with noticeable noise, while GFA performed the worst, with severe distortion of the image structure. Figure 6(b) illustrates the variation of the SSIM index with the number of training iterations for each algorithm. GAPT-Wavelet showed rapid improvement in the early stages, with the SSIM index quickly reaching 0.94, demonstrating excellent convergence speed and stability. Noise2Noise's SSIM index stabilized at 0.87, while the SSIM indices of WTFA and GFA stabilized at 0.725 and 0.517, respectively, indicating their denoising capabilities and convergence performance were significantly inferior to GAPT-Wavelet. Overall, GAPT-Wavelet demonstrated the best performance in both denoising accuracy and convergence speed. Next, MSE for the four algorithms was tested, and the results are shown in figure 7.

As shown in figure 7(a), at a Signal-to-Noise Ratio (SNR) of 10dB, the MSE of different algorithms gradually decreased as the number of iterations increased. The MSE of GAPT-Wavelet initially started at 0.16dB and rapidly dropped to

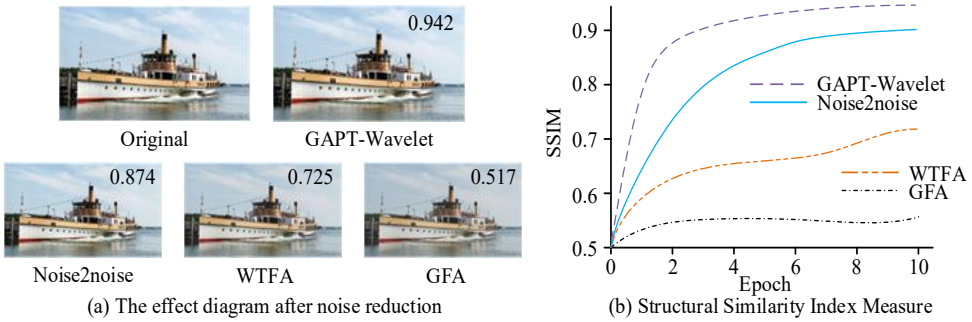

(a) The effect diagram after noise reduction (b) Structural Similarity Index Measure

Fig. 6. Comparison of SSIM index

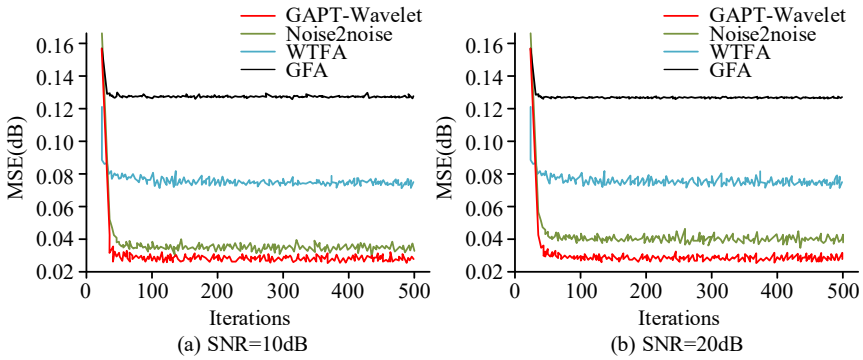

(a) SNR=10dB (b) SNR=20dB

Fig 7. Comparison of mean squared error

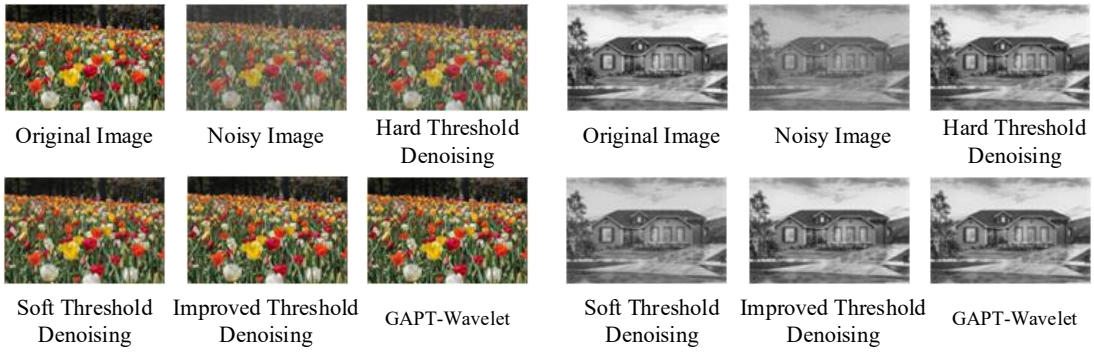

(a) Comparison of Different Thresholds: Flowers (b) Comparison of Different Thresholds: House

Fig.8 Comparison of denoising results

0.03dB within 50 iterations, after which it stabilized. Noise2Noise stabilized at 0.039dB. Figure 7(b) showed the situation at an SNR of 20dB. GAPT-Wavelet's MSE similarly dropped quickly from 0.16dB to 0.02dB, outperforming other algorithms by far. The MSE of WTFA and GFA stabilized at 0.078dB and 0.125dB, respectively. In terms of both initial decrease speed and final error values, GAPT-Wavelet demonstrated the best performance. Next, the denoising effects of the algorithms were experimentally verified, with the results shown in figure 8.

As shown in figure 8(a), GAPT-Wavelet not only effectively removed noise but also preserved the most complete details and color information, making it very close to the original image. In contrast, Hard Threshold Denoising caused excessive smoothing of image details, Soft Threshold Denoising yielded slightly better results but still showed some blurring, and Improved Threshold Denoising, while improving detail restoration, still lacked the naturalness in color and texture compared to GAPT-Wavelet. Figure 8(b) demonstrated the denoising performance comparison on a house image. GAPT-Wavelet again showed the best performance after denoising, clearly retaining the contours and textures of the house with almost no difference from the original image. In contrast, Hard Threshold Denoising blurred the edge details of the house, and although Soft Threshold Denoising and Improved Threshold Denoising restored some details, they still failed to completely eliminate the noise or over-smoothing problem. Further experimental verification provided more specific PSNR and MSE, as shown in table 1.

Table 1. PSNR and MSE comparison results

Image	Algorithms	PSNR (dB)	MSE (dB)
Flowers	GAPT-Wavelet	87.34	0.024
	Improved Threshold	78.57	0.063
	Soft Threshold	72.26	0.086
	Hard Threshold	69.64	0.145
	Nosie2nosie	84.85	0.037
	WTFA	77.59	0.078
	GFA	70.69	0.127
House	GAPT-Wavelet	87.9	0.023
	Improved Threshold	78.75	0.061
	Soft Threshold	72.38	0.091
	Hard Threshold	69.64	0.0145
	Nosie2nosie	84.48	0.032
	WTFA	77.24	0.075
	GFA	70.26	0.132

As shown in Table 1, in the flower image, the PSNR of GAPT-Wavelet was 87.34dB and the MSE was 0.024dB. Compared to Noise2Noise, the PSNR increased by 2.49dB and the MSE decreased by 35%. In the house image, GAPT-Wavelet had a PSNR of 87.90dB and an MSE of 0.021dB. Compared to WTFA and GFA, GAPT-Wavelet demonstrated significantly better denoising performance in both PSNR and MSE.

4.2 Verification of GAPT-Wavelet's computational efficiency and robustness

Based on the validation of GAPT-Wavelet's denoising performance, the study further assessed its computational efficiency and robustness. The experiment first examined the performance of the algorithms under different conditions and noise levels, while maintaining processing efficiency. The computation times for the four algorithms were first verified, as shown in figure 9.

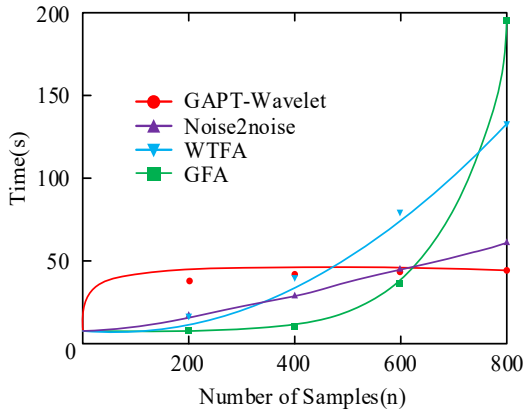

Fig. 9. Comparison of runtime under different sample size conditions

Figure 9 showed the runtime of four algorithms—GAPT-Wavelet, Noise2Noise, WTFA, and GFA—under different sample sizes. It could be seen that GAPT-Wavelet exhibited the smoothest growth in runtime. With n=200, its runtime was 8 seconds, and even with the maximum data size of n=800, its runtime was only 46 seconds, significantly lower than the other algorithms. In contrast, Noise2Noise took 67 seconds to run at n=800, while WTFA and GFA had even higher time complexities, with GFA's runtime approaching 200 seconds at n=800. Overall, GAPT-Wavelet maintained the lowest runtime across all data sizes, demonstrating extremely high computational efficiency and good scalability, making it the optimal choice among the four algorithms. The subsequent study compared the denoising performance of the algorithms under different interference conditions, as shown in figure 10.

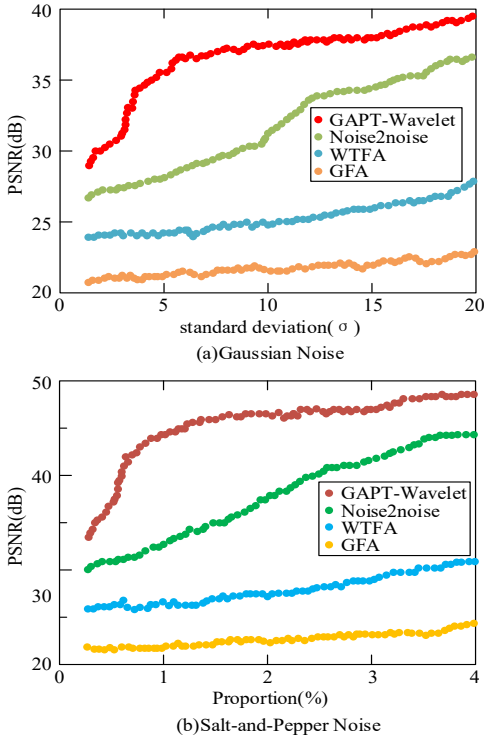

Fig. 10. Comparison of denoising performance under different interference conditions

In figure 10(a), a Gaussian noise scenario was presented, where GAPT-Wavelet consistently achieved the highest PSNR. Its initial value was close to 40dB and remained at 39dB even at σ=20, outperforming Noise2Noise at 36dB and WTFA at 28dB. In figure 10(b), a salt-and-pepper noise scenario was shown, where GAPT-Wavelet's initial PSNR was 36dB and remained at 48dB even with a 4% noise ratio. In comparison, GFA performed the worst, with a final PSNR of 24dB. Overall, GAPT-Wavelet demonstrated the lowest PSNR drop and strongest robustness in both noise scenarios, outperforming the other algorithms. The error rate of the algorithms was verified, with the results shown in figure 11.

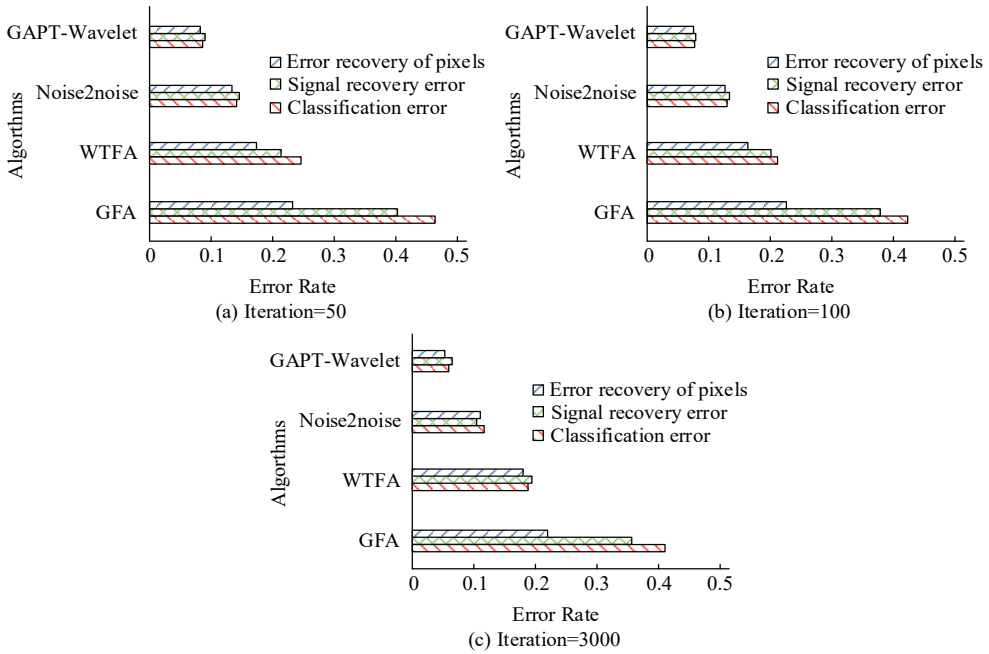

Fig. 11. Error rate comparison chart

In figure 11(a), it can be observed that, after 50 iterations, GAPT-Wavelet outperformed in all three error rates. The pixel recovery error rate was only 0.06, the signal recovery error rate was 0.065, and the classification error rate was less than 0.1, all lower than those of Noise2Noise. In figure 11(b), when the number of iterations increased to 100, GAPT-Wavelet's error rates further decreased, with the pixel recovery error rate at 0.056 and the classification error rate at 0.057, demonstrating exceptional convergence speed and stability. In figure 11(c), after 300 iterations, all three error rates of GAPT-Wavelet were below 0.05. In contrast, WTFA and GFA maintained relatively high error rates of 0.18 and 0.32, indicating poorer convergence performance. Overall, GAPT-Wavelet demonstrated the lowest error rates and optimal convergence across all iteration conditions. Finally, the study evaluates the denoising performance on different types of real-world engineering signals, and the results are presented in Table 2.

Table 2. Quantitative comparison of denoising performance on real-world engineering signals

Signal type	Method	SNR (dB)	MSE	Fault feature amplitude
Bearing-fault	Noisy	3.41	0.162	0.031
	WTFA	11.25	0.039	0.062
	Nosie2Noise	12.40	0.031	0.071
	GAPT-Wavelet	15.82	0.022	0.091
Gearbox-fault	Noisy	4.12	0.154	0.028
	WTFA	12.08	0.037	0.061
	Nosie2Noise	13.35	0.029	0.075
	GAPT-Wavelet	16.34	0.019	0.099
Motor-noise	Noisy	3.89	0.170	0.032
	WTFA	11.50	0.041	0.065
	Nosie2Noise	12.94	0.033	0.073
	GAPT-Wavelet	15.63	0.021	0.088

Table 2 presents the quantitative comparison of denoising performance for three types of real-world engineering signals, namely bearing fault vibration, gearbox fault vibration, and motor noise signals. For all signal types, GAPT-Wavelet consistently achieves the highest SNR and the lowest MSE among all compared methods. Notably, the amplitude of the extracted fault feature is significantly enhanced after denoising by GAPT-Wavelet, indicating that weak diagnostic information, which is hardly detectable in the original noisy signals, can be effectively recovered. Compared with traditional hard and soft thresholding as well as WTFA and Noise2Noise, the proposed method demonstrates superior denoising capability and better preservation of critical features. These results validate the robustness and practical value of GAPT-Wavelet for various technical diagnostic scenarios.

5. CONCLUSION

To address the issue of WTFA's poor performance in complex environments, a GAPT-Wavelet was proposed by combining FFDNet and GAN to improve the adaptive thresholding method. A nonlinear adaptive threshold function was also introduced to improve the traditional hard and soft threshold functions, leading to the design of GAPT-Wavelet. In denoising of floral images, GAPT-Wavelet achieved a PSNR of 87.34dB and an MSE of 0.024dB. For color images, it preserved the most complete details and color information. In the salt-and-pepper noise scenario, GAPT-Wavelet maintained a PSNR value of 48dB at a 4% noise level. After 300 iterations, GAPT-Wavelet's pixel recovery error rate was 0.043, the signal recovery error rate was 0.049, and the classification error rate was 0.045. The results demonstrated that GAPT-

Wavelet exhibited excellent denoising performance, showcasing outstanding denoising ability, fast convergence, and good preservation of details, especially in complex noise environments. Although GAPT-Wavelet performed well, its algorithm design was complex, and the computational resource consumption was relatively high. In scenarios with extremely large-scale data or real-time applications, there might be room for optimizing time efficiency. Future research could further optimize the computational efficiency of GAPT-Wavelet, combining lightweight models or hardware acceleration to better meet the demands of real-time processing and large-scale data applications, while also exploring its scalability in various complex noise scenarios.

Source of funding: *This research received no external funding.*

Author contributions: *Research concept and design, F.W.*

Declaration of competing interest: *The author declares no conflict of interest.*

REFERENCES

1. Wang Z, Li Z, Teng X, Chen D. LPMsDE: multi-scale denoising and enhancement method based on laplacian pyramid framework for forward-looking sonar image. IEEE Access. 202311(6):132942-132954. https://doi.org/10.1109/ACCESS.2023.3335372
2. Li Y, Ramli DA. Advances in time-frequency analysis for blind source separation; challenges, contributions, and emerging trends. IEEE Access. 2023;11(3):137450-137474. https://doi.org/10.1109/ACCESS.2023.3338024.
3. Ranjan R, Sahana BC, Bhandari AK. Cardiac artifact noise removal from sleep EEG signals using hybrid denoising model. IEEE Transactions on Instrumentation and Measurement. 2022;71(11):1-10. https://doi.org/10.1109/TIM.2022.3198441.
4. Cibira G, Glesk I, Dubovan J. SNR-based denoising dynamic statistical threshold detection of FBG spectral peaks. Journal of Lightwave Technology. 2022;41(8):2526-2539. https://doi.org/10.1109/JLT.2022.3229965.
5. Wei X, Feng G, Qi T, Guo J, Li Z. Reduce the noise of transient electromagnetic signal based on the method of SMA-VMD-WTD. IEEE Sensors Journal. 2022;22(15):14959-14969. https://doi.org/10.1109/JSEN.2022.3184697.
6. Hou Y, Liu R, Shu M, Xie X, Chen C. Deep neural network denoising model based on sparse representation algorithm for ecg signal. IEEE Transactions on Instrumentation and Measurement. 2023;72(4):1-11. https://doi.org/10.1109/TIM.2023.3251408.
7. Molaei AM, Fromenteze T, Skouroliakou V, Hoang TV, Kumar R, Fusco V, Yurduseven O. Development of fast Fourier-compatible image reconstruction for 3D near-field bistatic microwave imaging with dynamic metasurface antennas. IEEE Transactions on Vehicular Technology. 2022;71(12):13077-13090. https://doi.org/10.1109/TVT.2022.3201155
8. Jiang L, Shang W, Jiao Y, Xiang S. An adaptive generalized S-transform algorithm for seismic signal analysis. IEEE Access, 2022;10(7):127863-127870. https://doi.org/10.1109/ACCESS.2022.3227426.
9. Yuan H, Du R, Wang X, Wei X, Dai H. Advanced online broadband impedance spectrum acquisition of fuel cells by S-transform. IEEE Transactions on Industrial Electronics. 2022;70(4):3740-3750. https://doi.org/10.1109/TIE.2022.3177814.
10. Tian X, Zhu Q, Li Y, Wu M. Cross-domain joint dictionary learning for ECG inference from PPG. IEEE Internet of Things Journal. 2022;10(9: 8140-8154. https://doi.org/10.1109/JIOT.2022.3231862
11. Yao H M, Guo R, Li M, Jiang L, Ng MKP. Enhanced supervised descent learning technique for electromagnetic inverse scattering problems by the deep convolutional neural networks. IEEE Transactions on Antennas and Propagation. 2022; 70(8):6195-6206. https://doi.org/10.1109/TAP.2022.3196496.
12. Chen Y, Zhang D, Zhang H, Wang QG. Dual-path mixed-domain residual threshold networks for bearing fault diagnosis. IEEE Transactions on Industrial Electronics. 2022;69(12):13462-13472. https://doi.org/10.1109/TIE.2022.3144572.
13. Peng L, Guo A, Zhang S. Research on fault diagnosis method of High-Speed EMU air compressor based on ICEEMDAN and wavelet threshold combined noise reduction. IEEE Access. 2024;12(8):173484-173501. https://doi.org/10.1109/ACCESS.2024.3479721.
14. Wang X, Liu Z, Dai M, Li W, Tang J. Time-shift denoising combined with DWT-enhanced condition domain adaptation for motor bearing fault diagnosis via current signals. IEEE Sensors Journal. 2024;24(21):35019-35035. https://doi.org/10.1109/JSEN.2024.3455099.
15. Iqbal N. DeepSeg: Deep segmental denoising neural network for seismic data. IEEE Transactions on Neural Networks and Learning Systems. 2022;34(7): 3397-3404. https://doi.org/10.1109/TNNLS.2022.3205421.
16. Yao D, Zhou T, Yang J. Intelligent framework for bearing fault diagnosis in high-noise environments: A location-focused soft threshold denoising approach. IEEE Sensors Journal. 2024;24(7):9523-9535. https://doi.org/10.1109/JSEN.2024.3362349.
17. Li X, Chen J, Wang J, Li X and Kan Y. Research on fault diagnosis method of bearings in the spindle system for CNC machine tools Based on DRSN-Transformer. IEEE Access. 2024;12(4):74586-74595. https://doi.org/10.1109/ACCESS.2024.3404968.
18. Meng Y, Zhang J. A novel gray image denoising method using convolutional neural network. IEEE Access. 2022;10(4):49657-49676. https://doi.org/10.1109/ACCESS.2022.3169131
19. Yu W, Shen Y, He H, Yu X, Song S, Zhang J, Letalief KB. An adaptive and robust deep learning framework for THz ultra-massive MIMO channel estimation. IEEE Journal of Selected Topics in Signal Processing. 2023;17(4):761-776. https://doi.org/10.1109/JSTSP.2023.3282832.
20. Zhang K, Long M, Chen J, Liu M, Li J. CFPNet: A denoising network for complex frequency band signal processing. IEEE Transactions on Multimedia.

2023;25(3):8212-8224.
https://doi.org/10.1109/TMM.2022.3233398
21. Zhang K, Zuo W, Zhang L. FFDNet: Toward a fast and flexible solution for CNN-based image denoising. IEEE Transactions on Image Processing. 2018;27(9):4608-4622.
https://doi.org/10.1109/TIP.2018.2839891
22. Xu B, Zhou D, Li W. Image enhancement algorithm based on GAN neural network. IEEE Access. 2022; 10(3):36766-36777.
https://doi.org/10.1109/ACCESS.2022.3163241
23. Chen K, Kong Q, Dai Y, Xu Y, Yin F, Xu L, Cui S. Recent advances in data-driven wireless communication using gaussian processes: a comprehensive survey. China Communications. 2022;19(1):218-237.
https://doi.org/10.23919/JCC.2022.01.016.

Fan WANG obtained her ME in Electrical Engineering from Yanshan University in 2014. She currently works as a teacher at Shijiazhuang College of Applied Technology. Her main research direction is electrical engineering and vocational education.
e-mail:
mean_wangf@outlook.com